Equiaxed Dendritic Solidification with Convection: Part I. Multiscale/Multiphase Modeling

C.Y. WANG and C. BECKERMANN

Equiaxed dendritic solidification in the presence of melt convection and solid-phase transport is investigated in a series of three articles. In part I, a multiphase model is developed to predict composition and structure evolution in an alloy solidifying with an equiaxed morphology. The model accounts for the transport phenomena occurring on the macroscopic (system) scale, as well as the grain nucleation and growth mechanisms taking place over various microscopic length scales. The present model generalizes a previous multiscale/multiphase model by including liquid melt convection and solid-phase transport. The macroscopic transport equations for the solid and the interdendritic and extradendritic liquid phases are derived using the volume averaging technique and closed by supplementary relations to describe the interfacial transfer terms. In part II, a numerical application of the model to equiaxed dendritic solidification of an Al-Cu alloy in a rectangular cavity is demonstrated. Limited experimental validation of the model using a NH_4Cl-H_2O transparent model alloy is provided in part III.

I. INTRODUCTION

THE solidification microstructure of many metal alloys can generally be categorized into two groups: (1) columnar structures consisting of long, aligned dendrite arms that are attached to the mold wall; and (2) equiaxed structures consisting of crystals that grow radially inside an undercooled melt. In the recent past, columnar solidification with thermosolutal convection in the liquid melt and the resulting macrosegregation have been extensively studied.[2,3] In contrast, modeling of equiaxed dendritic solidification with convection has not been widely attempted because of the complications associated with the transport of free equiaxed crystals in the melt. The gravity-induced settling or flotation of free crystals is fundamental to the development and extent of the equiaxed zone and greatly affects the columnar to equiaxed transition. Moreover, grain transport may cause severe macrosegregation and structural inhomogeneities.

Toward predicting composition and structure in alloy castings, this article presents a general framework for modeling microstructure evolution during equiaxed alloy dendritic solidification. The modeling task is to incorporate descriptions of fundamental microscopic phenomena, such as nucleation, undercooling, and grain growth mechanisms, into macroscopic heat and fluid flow calculations. An extensive review of the micro-macroscopic modeling approach has been provided by Rappaz[4] and Thevoz *et al.*,[5] and recent developments have been reported in conference proceedings.[6,7] The two most recent approaches include the probabilistic modeling proposed by Brown and Spittle,[8] Zhu and Smith,[9] and Rappaz and Gandin[10] and the multiscale/multiphase model developed by Wang and Beckermann.[1,11,12] However, none of these previous models has considered melt convection and solid transport occurring during solidification, thereby greatly limiting their utility. The present work is intended to extend the multiphase model of Wang and Beckermann[1] by accounting for both melt convection and solid-phase transport. The present work is a continuation of Ni and Beckermann's two-phase modeling study,[13] which deals with globulitic solidification only but does account for melt convection and solid-phase transport.

The general multiscale/multiphase modeling framework is first introduced in Section II. A specific model obtained using the general approach is subsequently presented in Section III, where all the necessary supplementary relations are also supplied to complete the mathematical system. In the second article of this series on equiaxed dendritic solidification,[14] calculations for two-dimensional (2-D) equiaxed dendritic solidification of an Al-4 wt pct Cu alloy are carried out using the multiphase model, while a combined experimental and numerical investigation on the solidification of a NH_4Cl-H_2O alloy analog is reported in the third part of this series.[15]

II. MULTISCALE/MULTIPHASE MODELING

In this section, a micro-macroscopic model of dendritic alloy solidification is formulated by using a multiphase approach and volume averaging. After explaining the basic approach, the resulting macroscopic equations are summarized. The detailed derivation using the volume averaging technique can be found in Wang[16] and, for brevity, is not repeated here. Finally, the general forms of the constitutive relations for the phase interaction terms are presented.

A. *Multiphase Approach*

Consider a small volume element that contains several equiaxed dendritic crystals, as schematically illustrated in Figure 1, in which two different interfacial length scales can be distinguished. The solid crystal and the interdendritic liquid share a common interfacial structure of the order of 10^{-5} to 10^{-4} m, whereas the interface between the liquid

C.Y. WANG, Assistant Professor, is with the Department of Mechanical Engineering, University of Hawaii at Manoa, Honolulu, HI 96822. C. BECKERMANN, Associate Professor, is with the Department of Mechanical Engineering, The University of Iowa, Iowa City, IA 52242.

Manuscript submitted February 9, 1995.

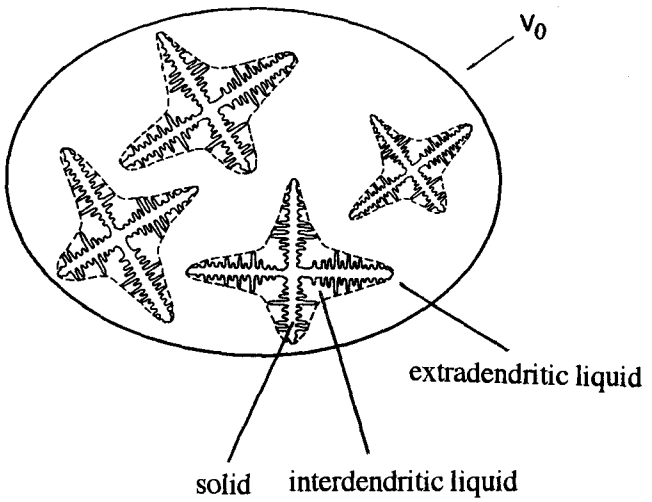

Fig. 1—Schematic illustration of the averaging volume and the dendrite envelope for equiaxed growth.

outside the grains and the interdendritic liquid has a higher length scale (of the order of 10^{-4} to 10^{-3} m). The size of the volume element is chosen such that it is much larger than all interfacial length scales but small compared to the system scale (of the order of 10^{-1} to 10^{0} m). Hence, a proper volume element could have a radius between 10^{-3} and 10^{-2} m, about the same size as a typical computational element used in numerical analyses.

The hypothetical interface between the interdendritic liquid and the liquid outside the crystals is referred to as the dendrite envelope.[17] The specification of this envelope is somewhat subjective. However, a reasonable choice appears to be a smooth surface connecting the primary and secondary dendrite arm tips, as shown by the interrupted line in Figure 1. More discussion on the envelope topology can be found in Wang and Beckermann.[1]

The volume element can be considered to consist of three different phases: the solid phase and the two liquid phases. The two liquid phases separated by the dendrite envelope are distinguished by their different interfacial length scales. Separate macroscopic conservation equations can then be formulated for each phase. These macroscopic equations are linked through interfacial transfer terms, which reflect the microscopic transport phenomena present at the interfaces. The new interface between the two liquid phases (*i.e.*, the envelope) thus provides an opportunity to incorporate additional microscopic phenomena in the model and to transmit information from the two different length scales into the macroscopic equations.

Based on the multiphase approach, the macroscopic conservation equations can be derived using the volume averaging technique, as described in Ni and Beckermann[13] and Wang and Beckermann.[1]

B. *Macroscopic Equations*

Application of certain averaging theorems to the microscopic (exact) conservation equations shown in the first column of Table I results in the macroscopic mass, momentum, energy, and species conservation equations for a phase k.[1,16] They are also summarized in Table I. The numerous symbols in Table I are defined in the Nomenclature.

Several features can be observed with regard to the averaged equations in Table I: (1) they contain the phase volume fraction, ε_k; (2) integrals arise over the interfacial areas, which account for the interactions of phase k with all other phases due to relative movement of interfaces (*e.g.*, phase change) and interfacial transport (*e.g.*, diffusion/convection); (3) they contain dispersive fluxes which reflect the effects of microscopic fluctuations of a property within a phase on the macroscopic transport (such terms are of key importance in turbulence modeling); and (4) an interfacial balance requires that the interfacial fluxes are equal on both sides of the interface. Since in the present model phases may be simply distinguished by their interfacial length scales, several interfacial integrals appear, through which information from each microscopic level is passed to the macroscopic level.

C. *Constitutive Relations*

The interfacial or phase interaction terms as well as the dispersive fluxes require further modeling, since the microscopic variables on which they are based are not known from the solution of the macroscopic equations. This information has been lost in the averaging process. The modeling of these terms for solidification systems requires (1) postulation of constitutive relations and (2) formal microscopic analyses for the system in question.

1. *Interfacial transfers due to interfacial/movement*

Interfacial movement can be due to phase change at the solid/liquid interface or dendrite tip advancement at the dendrite envelope. The exact expressions for the interfacial transfers of mass, momentum, heat, and species due to this movement are provided in Table I. Physically, these terms represent advection of an interfacial quantity of phase k due to the relative motion of the interface. In view of the mean value theorem for integrals, the terms can be modeled as the product of an interfacial area concentration and a mean interfacial flux. Hence, at the k-j interface, the interfacial mass-transfer rate becomes

$$\Gamma_{kj} = S_{kj}\,\rho_k \overline{w}_{nkj} \qquad [1]$$

where $\overline{w}_{nkj}$ represents the average normal velocity of the interface kj relative to phase k.

In a like manner, a general transfer Φ^{Γ}_{kj} corresponding to the property Ψ at the k-j interface due to interfacial movement can be expressed as

$$\Phi^{\Gamma}_{kj} = \overline{\Psi}_{kj}\,\Gamma_{kj} \qquad [2]$$

where the overbar together with the subscript kj denotes an average over the interfacial area A_{kj} in V_0. The term Φ^{Γ}_{kj} stands for the momentum transfer M^{Γ}_{kj}, heat transfer Q^{Γ}_{kj}, and species transfer J^{Γ}_{kj}, if Ψ corresponds to the velocity, enthalpy, and concentration, respectively. Note that Eq. [2] introduces interfacial quantities, $\overline{\Psi}_{kj}$, into the macroscopic conservation equations that are usually distinct from their volume averaged counterparts, $\langle\Psi_k\rangle^k$.

2. *Interfacial transfers due to diffusion/convection*

The exact expressions for the interfacial stress, M^{d}_{kj}, heat transfer, Q^{d}_{kj}, and species transfer, J^{d}_{kj}, due to diffusion/convection are also given in Table I. Physically, these terms represent the transport phenomena among the phases

Table I. Summary of Microscopic and Macroscopic Conservation Equations

	Microscopic Conservation Equations	Macroscopic Conservation Equations	Interfacial Balances	Dispersive Fluxes
Mass	$\frac{\partial}{\partial t}\rho_k + \nabla\cdot(\rho_k\mathbf{v}_k) = 0$	$\frac{\partial}{\partial t}(\varepsilon_k\rho_k) + \nabla\cdot(\varepsilon_k\rho_k\langle\mathbf{v}_k\rangle^k) = \sum_{j,j\neq k}\Gamma_{kj}$	$\Gamma_{kj} + \Gamma_{jk} = 0$	—
Momentum	$\frac{\partial}{\partial t}(\rho_k\mathbf{v}_k) + \nabla\cdot(\rho_k\mathbf{v}_k\mathbf{v}_k) = -\nabla p_k + \nabla\cdot\tau_k + \mathbf{b}_k$	$\frac{\partial}{\partial t}(\varepsilon_k\rho_k\langle\mathbf{v}_k\rangle^k) + \nabla\cdot(\varepsilon_k\rho_k\langle\mathbf{v}_k\rangle^k\langle\mathbf{v}_k\rangle^k) = -\varepsilon_k\nabla\langle p_k\rangle^k + \nabla\cdot(\langle\tau_k\rangle + \langle\tau_k^t\rangle) + \sum_{j,j\neq k}\mathbf{M}_{kj} + \varepsilon_k\langle\mathbf{b}_k\rangle^k$	$\mathbf{M}_{kj} + \mathbf{M}_{jk} = 0$	$\langle\tau_k^\wedge\rangle = -\langle\rho_k\hat{\mathbf{v}}_k\hat{\mathbf{v}}_k\rangle$
Energy	$\frac{\partial}{\partial t}(\rho_k h_k) + \nabla\cdot(\rho_k h_k\mathbf{v}_k) = -\nabla\cdot q_k$	$\frac{\partial}{\partial t}(\varepsilon_k\rho_k\langle h_k\rangle^k) + \nabla\cdot(\varepsilon_k\rho_k\langle h_k\rangle^k\langle\mathbf{v}_k\rangle^k) = -\nabla\cdot(\langle q_k\rangle + \langle q_k^t\rangle) + \sum_{j,j\neq k}Q_{kj}$	$Q_{kj} + Q_{jk} = 0$	$\langle q_k^\wedge\rangle = \langle\rho_k\hat{h}_k\hat{\mathbf{v}}_k\rangle$
Species	$\frac{\partial}{\partial t}(\rho_k C_k) + \nabla\cdot(\rho_k C_k\mathbf{v}_k) = -\nabla\cdot j_k$	$\frac{\partial}{\partial t}(\varepsilon_k\rho_k\langle C_k\rangle^k) + \nabla\cdot(\varepsilon_k\rho_k\langle C_k\rangle^k\langle\mathbf{v}_k\rangle^k) = -\nabla\cdot(\langle j_k\rangle + \langle j_k^t\rangle) + \sum_{j,j\neq k}J_{kj}$	$J_{kj} + J_{jk} = 0$	$\langle j_k^\wedge\rangle = \langle\rho_k\hat{C}_k\hat{\mathbf{v}}_k\rangle$

	Total Interfacial Transfers	Interfacial Transfers Due to Phase Change	Interfacial Stress and Transfers Due to Diffusion
Mass	Γ_{kj}	$\Gamma_{kj} = -\frac{1}{V_0}\int_{A_{kj}}\rho_k(\mathbf{v}_k - w_k)\cdot\mathbf{n}_k\,dA$	—
Momentum	$\mathbf{M}_{kj} = \mathbf{M}_{kj}^\Gamma + \mathbf{M}_{kj}^d$	$\mathbf{M}_{kj}^\Gamma = -\frac{1}{V_0}\int_{A_{kj}}\rho_k\mathbf{v}_k(\mathbf{v}_k - w_k)\cdot\mathbf{n}_k\,dA$	$\mathbf{M}_{kj}^d = \frac{1}{V_0}\int_{A_{kj}}\tau_k\cdot\mathbf{n}_k\,dA$
Energy	$Q_{kj} = Q_{kj}^\Gamma + Q_{kj}^d$	$Q_{kj}^\Gamma = -\frac{1}{V_0}\int_{A_{kj}}\rho_k h_k(\mathbf{v}_k - w_k)\cdot\mathbf{n}_k\,dA$	$Q_{kj}^d = -\frac{1}{V_0}\int_{A_{kj}}q_k\cdot\mathbf{n}_k\,dA$
Species	$J_{kj} = J_{kj}^\Gamma + J_{kj}^d$	$J_{kj}^\Gamma = -\frac{1}{V_0}\int_{A_{kj}}\rho_k C_k(\mathbf{v}_k - w_k)\cdot\mathbf{n}_k\,dA$	$J_{kj}^d = -\frac{1}{V_0}\int_{A_{kj}}j_k\cdot\mathbf{n}_k\,dA$

within V_0 and are caused by microscopic velocity, temperature, and species concentration gradients, on each side of the interface A_{kj}. Similar to the interfacial transfers due to interfacial movement, they can generally be modeled as the product of the interfacial area concentration S_{kj} and a mean interfacial flux. It can be assumed further that the mean interfacial flux, in turn, is linearly proportional to the difference between the interfacial average and the intrinsic volume average of a quantity of phase k, *i.e.*, $\overline{\Psi}_{kj} - \langle\Psi_k\rangle^k$. In other words, this difference is assumed to be the driving force for the interfacial flux. Hence, the interfacial mass transfer at the k-j interface due to diffusion/convection in phase k can be expressed as

$$J_{kj}^d = S_s\frac{D_k}{l_{kj}}(\overline{C}_{kj} - \langle C_k\rangle^k) \qquad [3]$$

where l is called the diffusion length, which characterizes the resistance to diffusion/convection.[1] The diffusion length is generally a complicated function of the microscopic phenomena, and its determination requires a formal microscopic analysis of the diffusion/convection processes (Section III–C–6 provides more detail).

3. *Modeling of macroscopic fluxes*

The macroscopic fluxes include the viscous stress $\langle\tau_k\rangle$, heat flux $\langle q_k\rangle$, and species flux $\langle j_k\rangle$, as well as their dispersive counterparts, $\langle\tau_k^t\rangle$, $\langle q_k^t\rangle$ and $\langle j_k^t\rangle$. These fluxes are typically modeled by introducing effective transport properties,[18] so that

$$\langle\Phi_k\rangle + \langle\Phi_k^t\rangle = -\Gamma_k^*\,\varepsilon_k\,\nabla\langle\Psi_k\rangle^k \qquad [4]$$

where Γ_k^* represents an overall macroscopic transport property, which is a function of not only the microscopic transport property but also the microstructure as well as microscopic flow fields. For multiphase flows, evaluation of these effective transport properties is an area of considerable research and controversy.[18]

III. A MULTIPHASE MODEL

The macroscopic conservation equations presented in Section II can be simplified for specific systems by making certain assumptions. Various limiting cases as well as simplified model equations for diffusion-controlled solidification have been extensively discussed by Wang and Beckermann.[1] As in Reference 1, the present study considers a three-phase system consisting of the solid ($k = s$), the interdendritic liquid ($k = d$), and the extradendritic liquid outside the dendrite envelope ($k = l$), so that $\varepsilon_s + \varepsilon_d + \varepsilon_l = 1$. An internal solid fraction can be defined as $\varepsilon_{si} = \varepsilon_s/(\varepsilon_s + \varepsilon_d)$, and the grain fraction is given by $\varepsilon_g = \varepsilon_s + \varepsilon_d$. It is further assumed that the solid (s) has only pointwise contact with the liquid (l) outside the dendrite envelope (Figure 1), so that

$$A_{sd} = A_{ds} = A_s,\ A_{dl} = A_{ld} = A_e, \text{ and } A_{sl} = A_{ls} = 0 \qquad [5]$$

These geometric relationships imply that there exists no direct coupling between phases (s) and (l), while phase (d) interacts with both phases (s) and (l). More model assumptions are made in Section A. Also, in the remainder of this article, the averaging symbols are dropped for convenience,

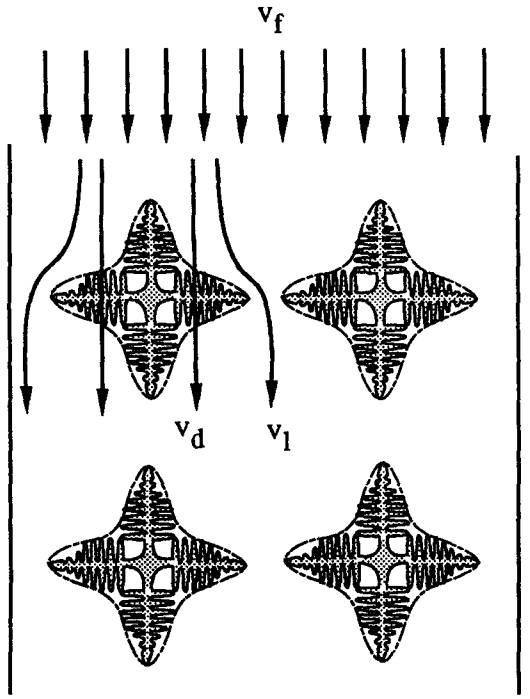

Fig. 2—Schematic of the partitioning of the liquid flow through the inter- and extradendritic regions in equiaxed solidification.[19]

namely, $\langle \Phi_k \rangle^k = \Phi_k$, whereas an interfacial quantity is still denoted by an overbar, so as to distinguish it from its volume-averaged counterpart.

A. *Model Assumptions*

The model equations presented subsequently are based on the following assumptions.

(1) Mechanical equilibrium exists, *i.e.*, $p_s = p_d = p_l = p$.
(2) The momentum exchange due to interfacial movement is neglected.
(3) A certain flow partitioning between the inter- and extradendritic regions is assumed, as originally proposed in Reference 19. As schematically shown in Figure 2, the liquid may flow either through the inter- or the extradendritic region. The relative portions can be quantified by introducing a flow partition tensor, κ_v, which is defined as the ratio of the liquid mass flux through the porous dendrites to the total liquid mass flux; *i.e.*,

$$\varepsilon_d \rho_d (\mathbf{v}_d - \mathbf{v}_s) = \kappa_v \, \varepsilon_f \rho_f (\mathbf{v}_f - \mathbf{v}_s) \qquad [6]$$

and

$$\varepsilon_l \rho_l (\mathbf{v}_l - \mathbf{v}_s) = (1 - \kappa_v) \, \varepsilon_f \rho_f (\mathbf{v}_f - \mathbf{v}_s) \qquad [7]$$

where ε_f and $\mathbf{v}_f$ stand for the total liquid fraction, consisting of the interdendritic and extradendritic phases, and the mixture velocity vector for both phases, respectively: $\varepsilon_f = \varepsilon_d + \varepsilon_l$ and $\varepsilon_f \rho_f \mathbf{v}_f = \varepsilon_d \rho_d \mathbf{v}_d + \varepsilon_l \rho_l \mathbf{v}_l$. Note that when $\kappa_v = \rho_d \varepsilon_d / (\rho_f \varepsilon_f)$, a uniform flow distribution results; *i.e.*, $\mathbf{v}_d = \mathbf{v}_l = \mathbf{v}_f$. The coefficient κ_v is also called the fluid collection efficiency of porous aggregates in chemical engineering.[20] A correlation for κ_v is developed in Section C. The concept of flow partitioning between the inter- and extradendritic regions is introduced to simplify the solution of the momentum equations in the proposed multiphase model. Once κ_v is calculated, only the momentum equation for the total liquid phase needs to be solved, and the individual liquid velocity fields, $\mathbf{v}_d$ and $\mathbf{v}_l$, can be algebraically obtained from Eqs. [6] and [7].

(4) Local thermal equilibrium exists, *i.e.*, $T_k = \overline{T}_{kj} = T$. The assumption can safely be made under normal solidification conditions because of the large value of the Lewis number of metal alloys, so that heat transfer at an interface is fast enough to reach local thermal equilibrium.
(5) The interdendritic liquid is well mixed so that $\overline{C}_{ds} = \overline{C}_{dl} = \overline{C}_{ld} = C_d = \overline{C}_e$. The assumption has been discussed in Wang and Beckermann[1] and found to be valid.
(6) The dendrite envelope is spherical.
(7) Thermophysical properties are the same for the interdendritic and extradendritic liquid phases.

As discussed in assumption 3, only the solid and total liquid phases require principal consideration. The distinction between the variables pertinent to the inter- and extradendritic liquids can be made algebraically after the primary variables pertinent to the total liquid phase (f) are obtained. The primary variables pertinent to the total liquid phase are defined by the rule-of-mixtures, *i.e.*,

volume fraction	$\varepsilon_f = \varepsilon_d + \varepsilon_l$	[8]
density	$\rho_f \varepsilon_f = \rho_d \varepsilon_d + \rho_l \varepsilon_l$	[9]
viscosity	$\rho_f \varepsilon_f \mu_f^* = \rho_d \varepsilon_d \mu_d^* + \rho_l \varepsilon_l \mu_l^*$	[10]
mass diffusivity	$\rho_f \varepsilon_f D_f^* = \rho_d \varepsilon_d D_d^* + \rho_l \varepsilon_l D_l^*$	[11]
thermal conductivity	$\varepsilon_f k_f^* = \varepsilon_d k_d^* + \varepsilon_l k_l^*$	[12]
specific heat	$\rho_f \varepsilon_f c_f = \rho_d \varepsilon_d c_d + \rho_l \varepsilon_l c_l$	[13]
concentration	$\rho_f \varepsilon_f C_f = \rho_d \varepsilon_d C_d + \rho_l \varepsilon_l C_l$	[14]
velocity	$\rho_f \varepsilon_f \mathbf{v}_f = \rho_d \varepsilon_d \mathbf{v}_d + \rho_l \varepsilon_l \mathbf{v}_l$	[15]

B. *Model Equations*

With the assumptions stated in Section A, a reduced set of model equations can be derived from the general formulation presented in Table I and the constitutive relations developed in Section II–C. These macroscopic equations are summarized in Table II. Some details of their derivations are described in Sections 1 through 5.

1. *Calculation of phase change rate*

As a critical parameter in solidification processes, the phase change rate Γ_s may be determined from the species balance in the interdendritic liquid phase (extracted from Table I):

$$\frac{\partial}{\partial t}(\rho_d \varepsilon_d C_d) + \nabla \cdot (\rho_d \varepsilon_d \mathbf{v}_d C_d) = \nabla \cdot (\rho_d \varepsilon_d D_d^* \nabla C_d) - \left[\overline{C}_{sd} \Gamma_s + \frac{\rho_s S_s D_s}{l_{sd}} (\overline{C}_{sd} - C_s)\right] + \left[\overline{C}_e \Gamma_e - \frac{\rho_l S_e D_l}{l_{ld}} (\overline{C}_e - C_l)\right] \qquad [16]$$

where the interfacial species fluxes on the right-hand side (RHS) have been replaced by their counterparts on the other

Table II. Summary of a Multiphase Model

Continuity Equations

Solid phase (s)

$$\frac{\partial}{\partial t}(\rho_s \varepsilon_s) + \nabla \cdot (\rho_s \varepsilon_s \mathbf{v}_s) = \Gamma_s$$

Total liquid phase (f)

$$\frac{\partial}{\partial t}(\rho_f \varepsilon_f) + \nabla \cdot (\rho_f \varepsilon_f \mathbf{v}_f) = -\Gamma_s$$

Interfacial Species Balance (for Calculating Phase Change Rate)

$$(\overline{C}_e - \overline{C}_{sd})\Gamma_s = \frac{\rho_s S_s D_s}{l_{sd}}(\overline{C}_{sd} - C_s) + \frac{\rho_l S_e D_l}{l_{ld}}(\overline{C}_e - C_l) + [\rho_d \varepsilon_d \frac{\partial \overline{C}_e}{\partial t} + \rho_d \varepsilon_d \mathbf{v}_d \cdot \nabla \overline{C}_e - \nabla \cdot (\rho_d \varepsilon_d D_d^* \nabla \overline{C}_e)]$$

Momentum Equations

Solid phase (s)

$$\frac{\partial}{\partial t}(\rho_s \varepsilon_s \mathbf{v}_s) + \nabla \cdot (\rho_s \varepsilon_s \mathbf{v}_s \mathbf{v}_s) = -\varepsilon_s \nabla p + \nabla \cdot (\mu_s^* \varepsilon_s \nabla \mathbf{v}_s) + \mathbf{M}_s^d + \rho_s \varepsilon_s \mathbf{g}$$

Total liquid phase (f)

$$\frac{\partial}{\partial t}(\rho_f \varepsilon_f \mathbf{v}_f) + \nabla \cdot (\rho_f \varepsilon_f \mathbf{v}_f \mathbf{v}_f) = -\varepsilon_f \nabla p + \nabla \cdot (\mu_f^* \varepsilon_f \nabla \mathbf{v}_f) - \mathbf{M}_s^d + \varepsilon_f \rho_f \mathbf{g} + \nabla \cdot [\gamma \rho_f \varepsilon_f (\mathbf{v}_f - \mathbf{v}_s)(\mathbf{v}_f - \mathbf{v}_s)]$$

Species Equations

Solid phase (s)

$$\frac{\partial}{\partial t}(\rho_s \varepsilon_s C_s) + \nabla \cdot (\rho_s \varepsilon_s \mathbf{v}_s C_s) = \nabla \cdot (\rho_s \varepsilon_s D_s^* \nabla C_s) + \overline{C}_{sd}\Gamma_s + \frac{\rho_s S_s D_s}{l_{sd}}(\overline{C}_{sd} - C_s)$$

Total liquid phase (f)

$$\frac{\partial}{\partial t}(\rho_f \varepsilon_f C_f) + \nabla \cdot (\rho_f \varepsilon_f \mathbf{v}_f C_f) = \nabla \cdot (\rho_f \varepsilon_f D_f^* \nabla C_f) - [\overline{C}_{sd}\Gamma_s + \frac{\rho_s S_s D_s}{l_{sd}}(\overline{C}_{sd} - C_s)] + \nabla \cdot \{\rho_f \varepsilon_f (\mathbf{v}_f - \mathbf{v}_s)[C_f - \kappa_v C_d - (1-\kappa_v)C_l]\}$$

Mixture Energy Equation

$$\frac{\partial}{\partial t}[(\rho_s \varepsilon_s c_s + \rho_f \varepsilon_f c_f)T] + \nabla \cdot [(\rho_s \varepsilon_s c_s \mathbf{v}_s + \rho_f \varepsilon_f c_f \mathbf{v}_f)T] = \nabla \cdot [(\varepsilon_s k_s^* + \varepsilon_f k_f^*)\nabla T] + \Gamma_s[\Delta h + (c_s - c_l)T_E]$$

Auxiliary Relations for Secondary Variables

Interdendritic liquid fraction

$$\frac{\partial}{\partial t}(\rho_d \varepsilon_d) + \nabla \cdot (\rho_d \varepsilon_d \mathbf{v}_d) = S_e \rho_l \overline{w}_{ne} - \Gamma_s$$

Extradendritic liquid fraction

$$\varepsilon_l = \varepsilon_f - \varepsilon_d$$

Extradendritic liquid concentration

$$C_l = (\rho_f \varepsilon_f C_f - \rho_d \varepsilon_d \overline{C}_e)/(\rho_l \varepsilon_l)$$

Inter- and extradendritic liquid velocities

$$\mathbf{v}_d = \mathbf{v}_s + \kappa_v \frac{\rho_f \varepsilon_f}{\rho_d \varepsilon_d}(\mathbf{v}_f - \mathbf{v}_s);\ \mathbf{v}_l = \mathbf{v}_s + (1-\kappa_v)\frac{\rho_f \varepsilon_f}{\rho_l \varepsilon_l}(\mathbf{v}_f - \mathbf{v}_s)$$

sides of the interfaces, because the former become indeterminate under assumption 5.

Eliminating Γ_e in Eq. [16] using the mass conservation equation for phase (d) and noting that $C_d = \overline{C}_e$ (assumption 5), it follows that

$$(\overline{C}_e - \overline{C}_{sd})\Gamma_s = \frac{\rho_s S_s D_s}{l_{sd}}(\overline{C}_{sd} - C_s) + \frac{\rho_l S_e D_l}{l_{ld}}(\overline{C}_e - C_l) + [\rho_d \varepsilon_d \frac{\partial \overline{C}_e}{\partial t} + \rho_d \varepsilon_d \mathbf{v}_d \cdot \nabla \overline{C}_e - \nabla \cdot (\rho_d \varepsilon_d D_d^* \nabla \overline{C}_e)] \quad [17]$$

Physically, this equation implies that the species flux rejected into the interdendritic liquid due to phase change (left-hand side (LHS)) is either diffused/convected into the solid and extradendritic liquid through interphase exchanges within the control volume (the first and second terms on the RHS), is stored in the interdendritic region (third term on the RHS), or is advected and diffused out of the control volume (fourth and fifth terms on the RHS). Equation [17] is used to calculate the phase change rate, Γ_s.

2. *Momentum conservation*

The momentum equation for phase (f) listed in Table II is obtained by summing up the momentum conservation equations for phases (d) and (l), as listed in Table I, as well as using assumption 3 stated in Section A. The viscous

terms are linear so that they are additive, whereas the summation of the nonlinear advective terms results in an additional term (the last term on the RHS), where γ is called the momentum dispersion coefficient and is given by[16]

$$\gamma = 1 - \rho_f \varepsilon_f \left[\frac{\kappa_v^2}{\rho_d \varepsilon_d} + \frac{(1-\kappa_v)^2}{\rho_l \varepsilon_l} \right] \quad [18]$$

When $\kappa_v = \rho_d \varepsilon_d / \rho_f \varepsilon_f$ (*i.e.*, uniform flow through the inter- and extradendritic regions), $\gamma = 0$ so that the last term in the momentum equation for phase (f) vanishes. This is why γ is called the dispersion coefficient.

The solid/liquid interfacial drag, M_s^d, in the two momentum equations listed in Table II is modeled in Section III–C–4.

3. *Species conservation*

The species conservation equations for the solid and total liquid phases can be derived in a similar fashion. These equations contain interfacial species transfer terms that are inversely proportional to the solid and liquid diffusion lengths l_{sd} and l_{ld}, respectively. These diffusion lengths are modeled in Section III–C–6. Notice again that when $\kappa_v = \varepsilon_d \rho_d / (\varepsilon_f \rho_f)$ (uniform flow), the last term in the species conservation equation for the total liquid phase drops out.

4. *Energy conservation*

In deriving the energy equation for the multiphase mixture, the macroscopic enthalpies of the various phases are expressed as linear functions of temperature:

$$h_s = c_s T \quad [19]$$

$$h_d = c_d T + (c_s - c_d) T_E + \Delta h \quad [20]$$

and

$$h_l = c_l T + (c_s - c_l) T_E + \Delta h \quad [21]$$

where Δh is the latent heat of fusion at the eutectic temperature, T_E; *i.e.*,

$$\Delta h = (h_l - h_s)|_{T=T_E} \quad [22]$$

The last term on the RHS of the energy equation listed in Table II represents the latent heat release due to solidification.

5. *Secondary variables*

The model equations listed in Table II constitute a complete mathematical formulation for eight primary variables: ε_s, Γ_s, $\mathbf{v}_s$, $\mathbf{v}_f$, p, C_s, C_f, and T, while the total liquid fraction, ε_f, can be obtained from the constraint $\varepsilon_s + \varepsilon_f = 1$. All quantities pertinent to the inter- and extradendritic liquid phases are classified as secondary variables whose determination from the preceding primary variables is explained subsequently.

To distinguish the inter- and extradendritic liquid fractions from the total liquid fraction ε_f, one can resort to the following mass conservation equation for the interdendritic liquid phase:

$$\frac{\partial}{\partial t}(\rho_d \varepsilon_d) + \nabla \cdot (\rho_d \varepsilon_d v_d) = \Gamma_e - \Gamma_s \quad [23]$$

where Γ_e is related to the growth velocity of the dendrite envelope *via* Eq. [1]:

$$\Gamma_e = S_e \rho_l \overline{w}_{ne} \quad [24]$$

Hence, the quantity Γ_e can be calculated from the growth model for the dendrite envelope, which is provided in Section III–C–3. Once ε_d is obtained, the extradendritic liquid fraction is simply equal to $(\varepsilon_f - \varepsilon_d)$.

By definition, the extradendritic liquid concentration can be calculated, once C_f is available, from

$$C_l = (\rho_f \varepsilon_f C_f - \rho_d \varepsilon_d \overline{C}_e)/(\rho_l \varepsilon_l) \quad [25]$$

where the relation $C_d = \overline{C}_e$ has been used due to the assumption that the interdendritic liquid is well mixed, namely, assumption 5.

Likewise, the liquid velocities in the inter- and extradendritic regions are obtained, respectively, from the definition of the flow partition coefficient:

$$\mathbf{v}_d = \mathbf{v}_s + \kappa_v \frac{\rho_f \varepsilon_f}{\rho_d \varepsilon_d} (\mathbf{v}_f - \mathbf{v}_s) \quad [26]$$

$$\mathbf{v}_l = \mathbf{v}_s + (1-\kappa_v) \frac{\rho_f \varepsilon_f}{\rho_l \varepsilon_l} (\mathbf{v}_f - \mathbf{v}_s) \quad [27]$$

in which κ_v is calculated, as shown in Section III–C–4.

The preceding auxiliary relations for calculating the secondary variables from the primary variables are also summarized in Table II. To complete the mathematical system, however, supplementary relations are needed for the interfacial area concentrations, S_s and S_e, the growth velocity of dendrite envelope, $\overline{w}_{ne}$, the solid/liquid interfacial drag, M_s^d, the flow partition coefficient, κ_v, the interfacial diffusion lengths, l_{sd} and l_{ld}, and the macroscopic transport properties. These additional inputs to the multiphase model are provided in Section C.

C. *Supplementary Relations*

1. *Morphological relations*

The interfacial area concentrations, S_s and S_e, characterize the topology of the interfacial structures and thus are related to complex microscopic phenomena, such as the growth of various solid microstructures, impingement of interfaces, and coarsening of dendrite arms. The area concentrations also play important roles in the modeling of the interfacial transfer terms, as shown in Section B. For completeness, the morphological relations derived by Wang and Beckermann[1] for an equiaxed morphology are included in Table III. They are based the assumption of a platelike geometry of the dendrite arms and an equivalent sphere concept for the dendrite envelope. The interfacial area concentrations in Table III are expressed as functions of the traditionally employed secondary dendrite arm spacing and the grain density. The interfacial area concentration, S, is related to the specific area, S_v, by $S = S_v(1 - \varepsilon)$, where ε is the volume fraction of the microstructure under consideration. For more details on the derivation of these morphological relations and their underlying assumptions, the reader is urged to consult Wang and Beckermann.

2. *Grain nucleation*

As an important microstructural parameter, the grain density is needed for the evaluation of certain geometric quantities listed in Table III. Due to solid motion in the equiaxed case, this grain density, n, is not only determined by nucleation mechanisms but also modified by the flow field

Table III. Summary of Morphological Relations for Equiaxed Crystals[1]

Mean diameter of the solid phase, d_s	$\frac{\varepsilon_s \lambda_2}{1-\varepsilon_l}$
Mean diameter of the dendrite envelope, d_e	$\left(\frac{6(1-\varepsilon_l)}{n\pi}\right)^{1/3}$
Solid/interdendritic liquid interfacial area concentration, S_s	$\frac{2}{\lambda_2}$
Envelope area concentration, S_e	$\frac{1}{\phi_e}(36\pi)^{1/3} n^{1/3}(1-\varepsilon_l)^{2/3}$

during solidification, according to the following conservation equation:[13]

$$\frac{\partial n}{\partial t} + \nabla \cdot (\mathbf{v}_s n) = \dot{n} \qquad [28]$$

where the second term on the LHS is the flux of grains due to a finite solid velocity, $\mathbf{v}_s$. The term $\dot{n}$ is the net nucleation rate accounting for both the birth and death of grains due to heterogeneous nucleation, remelting, dendrite arm pinch-off, agglomeration, and other effects. Although a number of semiempirical nucleation models are available, they do not explicitly account for fragmentation and agglomeration effects in the presence of convection. The realistic modeling of grain structure formation on the macroscopic scale will largely depend on resolving these issues. Careful experimentation coupled with solutions of the present model equations may help in this respect.

As a first approximation, the calculations presented in parts II and III of this study employ the simplest nucleation model, namely, the instantaneous nucleation law proposed by Stefanescu *et al.*[21] In this model, it is assumed that a certain number of nuclei instantaneously appear as soon as the temperature of the liquid melt falls below the nucleation temperature, T_N; *i.e.*, $\dot{n} = n_0 \delta(T - T_N)$, where n_0 is a constant and δ is the Dirac delta function. Moreover, nucleation can only occur if the local grain density before nucleation is equal to zero. This implies that no new grains will nucleate in the immediate neighborhood of existing grains. In the presence of solid movement, grains may be advected into regions of higher temperature and remelt to a sufficiently small diameter d_{si}. In this case, death of the grains takes place, and the present nucleation model instantaneously resets the local grain density to zero. The control volume in question is then allowed to renucleate later when the conditions are right. Grains may exist in regions of superheated melt as long as their diameter is above d_{si}. Again, such a model can only be expected to capture some of the first-order effects of the grain density on the growth and transport phenomena, and future work should concentrate on explicitly including the fragmentation/agglomeration effect.

3. *Grain growth*

The dendrite envelope motion is governed by the growth of dendrite tips. The growth model for dendrite tips can be obtained by connecting two phenomena: solute transport near the tip and tip stability. Assuming no back diffusion in the solid and using the common marginal stability condition for tip growth, as proposed by Lipton *et al.*,[22] it can be shown that[23]

$$\overline{w}_{ne} = \frac{4\sigma^* D_l m(\kappa-1)\overline{C}_e}{\Gamma} \mathrm{Pe}_t^2 \qquad [29]$$

where σ^* is the stability constant ($\approx 1/4\pi^2$ in the pure diffusion limit) and Γ is the Gibbs–Thomson coefficient. The tip Peclet number, Pe_t, is related to the dimensionless solutal undercooling, Ω:

$$\Omega = \frac{\overline{C}_e - C_l}{\overline{C}_e(1-\kappa)} \qquad [30]$$

via the solution of the solute transport problem near the tip. Coupling such a solution with Eq. [29] yields a growth model that relates $\overline{w}_{ne}$ directly to the solutal undercooling Ω. Equation [29] is generic, in that all of the effects of the assumed dendrite tip shape and flow conditions around the tips are incorporated in the stability constant σ^* and the relation between the tip Peclet number Pe_t and the undercooling Ω. Subsequently, diffusion- and convection-dominated cases are considered, separately.

For diffusion-dominated growth, the exact Ivantsov function is given by

$$\mathrm{Iv}(\mathrm{Pe}_t) = \mathrm{Pe}_t \exp(\mathrm{Pe}_t) E_1(\mathrm{Pe}_t) = \Omega \qquad [31]$$

where $E_1(\mathrm{Pe}_t)$ is the exponential integral function. For computational convenience, the inverse Ivantsov function can be approximated by[1]

$$\mathrm{Pe}_t = \mathrm{Iv}^{-1}(\Omega) = a\left(\frac{\Omega}{1-\Omega}\right)^b \qquad [32]$$

where $a = 0.4567$ and $b = 1.195$ give the best fit. Substitution of Eq. [32] into Eq. [29] and insertion of $\sigma^* = 1/4\pi^2$ yield a growth model for diffusion-dominated dendrite tip growth. This model has been used in Wang and Beckermann[1,12] for diffusion-dominated solidification.

For convection-dominated growth, there is ample experimental evidence showing that both the stability criterion and the species gradients are affected by the flow field around dendrite tips.[24] A reliable and accurate model accounting for these convection effects, however is not yet available. To a first approximation, one can assume a negligible influence of convection on the stability criterion, and thus the focus is first placed on the fluid flow effect on the species transport field around dendrite tips.

Considerable research has been conducted in order to find analytical solutions of the heat transport around dendrite tips in the presence of convection. A summary has been given by Ananth and Gill.[25] It was found that the Stokes approximation of the Navier–Stokes equations for convection in a subcooled melt yields an exact solution for shape preserving growth of a parabolic dendrite. The solution was also found to be in good agreement with the available experimental data of Huang and Glicksman.[24] In terms of the tip Peclet number Pe_t and the dimensionless undercooling Ω, this solution can be written as

$$\Omega = 2\mathrm{Pe}_t \left(\int_1^\infty \frac{\exp\left[-\int_1^\eta (f/\eta)d\eta\right]}{\eta} d\eta \right) \qquad [33]$$

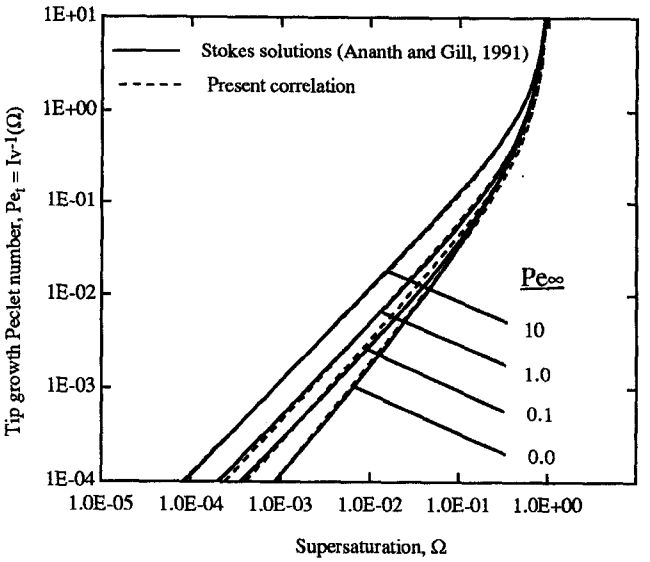

Fig. 3—Comparison of the Stokes' solution of Ananth and Gill,[25] for Sc > 20, with the present correlation, Eqs. [32] and [36], for dendrite tip growth.

where the function $f(\eta)$ is given by

$$f(\eta) = 2\mathrm{Pe}_t\,\eta^2 + \frac{2\mathrm{Pe}_\infty}{E_1[(\mathrm{Pe}_\infty + 2\mathrm{Pe}_t)/\mathrm{Sc}]}\,[\eta^2(2\ln\eta - 1) + 1] \quad [34]$$

and the ambient Peclet number is based on the relative velocity between the liquid and the solid dendrite; *i.e.*,

$$\mathrm{Pe}_\infty = |\mathbf{v}_l - \mathbf{v}_s| R_t/D_l \quad [35]$$

In Eqs. [33] through [35], the heat-transfer solution of Reference 23 has been rewritten in terms of mass-transfer quantities, *i.e.*, the solutal Peclet numbers and the Schmidt number, Sc. Parametric calculations indicate that the analytical solution given by Eqs. [33] and [34] becomes independent of the Schmidt number when Sc is greater than about 20, which is the case for all metal and transparent model (*e.g.*, NH_4Cl-H_2O) alloys. When $\mathrm{Pe}_\infty = 0$, which implies no convection, Eq. [34] yields $f(\eta) = 2\mathrm{Pe}_t\eta^2$ and Eq. [33] reduces to the Ivantsov solution for pure diffusion, as given in Eq. [31].

Again, for computational efficiency, the inverse of the solution to Eqs. [33] and [34] for convection-dominated dendrite tip growth can be curve fitted, for Sc > 20, using the same form as Eq. [32]:

$$a = 0.4567 + 0.173\,\mathrm{Pe}_\infty^{0.55} \quad [36a]$$

$$b = 1.195 - 0.145\,\mathrm{Pe}_\infty^{0.16} \quad [36b]$$

Figure 3 shows a comparison of the present correlation consisting of Eqs. [32] and [36] with the Stokes solution given by Eqs. [33] and [34] for various values of Pe_∞. It can be seen that the present correlation adequately matches with the analytical results for Sc > 20.

4. *Solid/liquid interfacial drag*

The dissipative interfacial stress in a particulate system has traditionally been modeled using various approaches. For high solid fractions (*i.e.*, the packed bed regime), the porous medium approach is often adopted, with the permeability representing a key parameter;[26,27] while at low solid fractions (*i.e.*, the free particle regime), the submerged object model is more frequently used in which the drag coefficient is important.[28] Recently, both approaches have been unified by Wang *et al.*[19] for the multiparticle system of equiaxed solidification, and a general correlation (valid for all solid fractions ranging from zero to unity) for the dissipative interfacial stress, M_s^d, on the solid crystals in the Stokes regime has been obtained; *i.e.*,

$$\mathbf{M}_s^d = \varepsilon_f \beta^2 \frac{\mu_f}{R_e^2}\,\varepsilon_f(\mathbf{v}_f - \mathbf{v}_s) \quad [37]$$

where β is a dimensionless parameter, which is only a function of the particle volume fraction and its morphology, and R_e is the envelope radius. The expression for β is given by[19]

$$\beta = \frac{\beta_d}{[(1-\varepsilon_l)^n + (\beta_d/\beta_l)^{2n}]^{1/2n}} \quad [38]$$

where

$$\beta_d = \frac{3\sqrt{5}}{(1-\varepsilon_{si})^{3/2}}\frac{S_s}{\phi_e S_e} \quad [39]$$

$$\beta_l = \left\{\frac{9}{2}(1-\varepsilon_l)\frac{2 + 4/3(1-\varepsilon_l)^5}{2-3(1-\varepsilon_l)+3(1-\varepsilon_l)^5-2(1-\varepsilon_l)^6}\right.$$
$$\left.\frac{1}{C_p(\phi_e)}\frac{2\beta_d^2(1-\tanh\beta_d/\beta_d)}{2\beta_d^2 + 3(1-\tanh\beta_d/\beta_d)}\right\}^{1/2} \quad [40]$$

$$n = 0.176\log\beta_d + 0.275 \quad [41]$$

The function $C_p(\phi_e)$ accounts for the effect of an aspherical dendrite envelope, with ϕ_e being the sphericity of the dendrite envelope.[29,1] The following expression for $C_p(\phi_e)$ has been proposed by Wang *et al.*:[19]

$$C_p(\phi_e) = \begin{cases} \phi_e^2 & \text{for } 0.7 > \varepsilon_l > 0.0 \\ 1.26\log_{10}\left(\dfrac{\phi_e}{0.163}\right) & \text{for } 1 > \varepsilon_l > 0.7 \end{cases} \quad [42]$$

While other details on the drag model are available elsewhere,[19] several salient features of the model are outlined here. First, note that this drag model accounts for the multiple length scales present in a dendritic structure, namely, S_s and S_e (or R_e). Second, the drag model encompasses many important limiting cases, which include the single equiaxed dendrite[29,30] and packed beds of impermeable and permeable spheres. Third, the model has been validated against various experimental data available in the literature for both globular and dendritic crystals.[19] In particular, it was found that this model improves the prediction of permeabilities of equiaxed dendritic structures due to its explicit consideration of multiple length scales. For spherical solid particles, this drag model reduces identically to the well-known Stokes' law for the drag coefficient in the free particle regime,[28] while it coincides with the Kozeny–Carman permeability relation in the packed bed regime.

5. *Flow partitioning between inter- and extradendritic regions*

In equiaxed solidification, it can be assumed that the flow partition coefficient is isotropic, so that only a single value

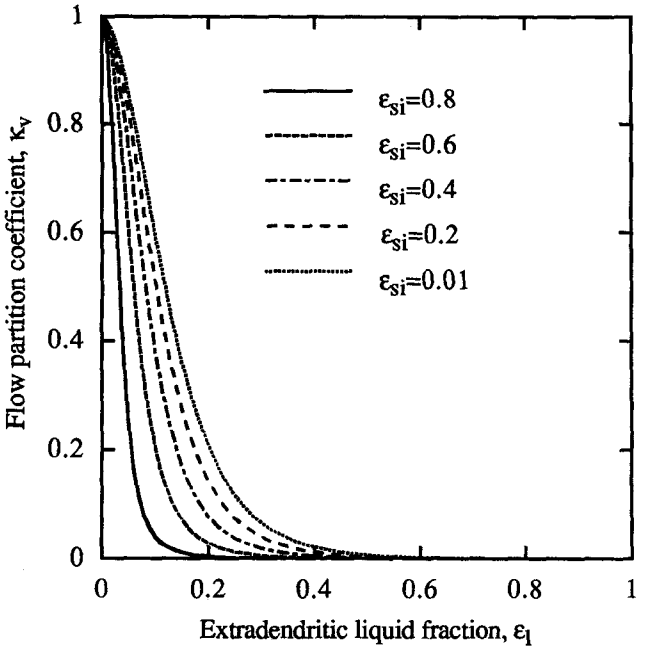

Fig. 4—Flow partition coefficients as functions of the extradendritic liquid fraction and internal solid fraction for $S_s/S_e = 0.1$.[19]

of κ_v is required. It has been shown by Wang *et al.*[19] that

$$\kappa_v = (1 - \varepsilon_l)(\beta/\beta_d)^2 \qquad [43]$$

where β and β_d are given by Eqs. [38] and [39]. Figure 4 illustrates the effects of the extradendritic liquid fraction, ε_l, and internal solid fraction, ε_{si} (*i.e.*, the ratio of the solid fraction to the grain fraction), on the flow partition coefficient in an equiaxed dendritic system with $S_s/S_e = 0.1$. As can be seen, the portion of the flow through the dendrites approaches zero in the free particle regime (*i.e.*, higher ε_l). On the other hand, in the packed bed regime, the flow partition coefficient quickly increases as ε_l decreases and reaches unity at $\varepsilon_l = 0$, at which point all flow must be through the interdendritic spaces.

6. *Interfacial mass transfer*

By considering the diffusion process in the solid and the moving solid/liquid interface due to phase change, it has been shown by Wang and Beckermann[1] that the solid diffusion length l_{sd} in dendritic solidification is given by

$$l_{sd} = d_s/6 \qquad [44]$$

where the mean diameter of the solid phase, d_s, can be related to the secondary dendrite arm spacing, λ_2, and the volume fraction ε_s (Table III).

In the presence of convection, the diffusion length ahead of the dendrite envelope in equiaxed solidification can be expressed as[16]

$$\frac{d_e}{l_{ld}} = 2 + 0.865 \left(\frac{C_\varepsilon}{\varepsilon_l}\right)^{1/3} \mathrm{Pe}_\varepsilon^{1/3} \qquad [45]$$

where

$$\mathrm{Pe}_\varepsilon = \frac{\varepsilon_l |\mathbf{v}_l - \mathbf{v}_s| d_e}{D_l} \qquad [46]$$

and

$$C_\varepsilon = \frac{2 + \frac{4}{3}(1-\varepsilon_l)^{5/3}}{2 - 3(1-\varepsilon_l)^{1/3} + 3(1-\varepsilon_l)^{5/3} - 2(1-\varepsilon_l)^2} \qquad [47]$$

This correlation is based on the momentum–mass-transfer analogy and is derived along the same lines as the interfacial drag expressions given by Eqs. [37] through [42]. A comparison between this correlation and Agarwal's formula,[31] which was employed previously by Ni and Beckermann,[32] indicated a discrepancy of less than 20 pct for all solid fractions.[16] In addition, it should be mentioned that the correlation given by Eqs. [45] through [47] neglects the effect of interfacial movement. This can be justified by the fact that in the presence of convection, the convection effect dominates that of interfacial movement in determining mass-transfer rates. Overall, the use of the preceding correlation should only be viewed as a first attempt, based on a review of the literature available on convective heat/mass transfer in multiparticle systems,[16] at estimating the convective mass-transfer rate for equiaxed dendritic crystals. Experiments are underway to directly measure the mass-transfer coefficient for growing equiaxed crystals.[33]

7. *Macroscopic transport properties*

The effective macroscopic viscosities μ_s^* and μ_l^* represent the rheological behavior of a multiphase mixture. They are dependent on the viscous properties and deformations of the phases, the flow field, and the distribution and geometry of the dispersed or suspended phase. To a first approximation, the liquid macroscopic viscosity can be taken to be equal to its microscopic counterpart, *i.e.*,

$$\mu_l^* = \mu_l \qquad [48]$$

Modeling of the macroscopic viscosity for the solid phase must account for the packing limit, where the equiaxed grains impinge upon each other (*i.e.*, when $\varepsilon_g = \varepsilon_g^c$) and form a coherent and rigid solid structure. In this limit, μ_s^* must approach an infinite value so that the macroscopic velocity gradients of the solid phase vanish. If the rigid solid is fixed to a wall, the solid velocity will then be uniformly equal to the velocity of the wall (which may be zero).

In the other extreme, where $\varepsilon_g \to 0$, the seminal theory of Einstein predicts that $\mu_s^* = 3.5\ \mu_l$.[34] In solidification systems, where the grain fraction may vary anywhere from zero to unity, a smooth transition between these two limits is necessary. Based on the model of Krieger[35] and as Ni and Beckermann[32] did, we use the following formula for μ_s^*:

$$\mu_s^* = \frac{\mu_l}{\varepsilon_g} [(1 - \varepsilon_g/\varepsilon_g^c)^{-2.5\varepsilon_g^c} - (1 - \varepsilon_g)] \qquad [49]$$

Note that the RHS of Eq. [49] reduces to $3.5\ \mu_l$ for $\varepsilon_g \to 0$ and to an infinite value for $\varepsilon_g = \varepsilon_g^c$. It should also be emphasized that for dendritic structures, the solid viscosity is not directly dependent on the solid fraction but rather on the grain fraction. In other words, as soon as the grain fraction reaches the packing limit (ε_g^c is about 0.637), the solid microstructure will become rigid, even though the solid fraction may be much lower than ε_g^c. There has been ample experimental evidence to support this hypothesis. For ex-

ample, experimental data for different alloys[36,37] indicated that the packing limit could be reached at solid fractions between 0.1 and 0.3 in a large-grained casting, where the grain fraction is much higher than the solid fraction. In contrast, in well-grain-refined castings, packing of dendrites ("dendrite coherency") was found to occur at much higher solid fractions between 0.5 and 0.65. This is because the grain fraction is nearly equal to the solid fraction for small grains.

As a first approximation, the macroscopic thermal conductivity and mass diffusivity are taken to be equal to their microscopic counterparts:

$$k_k^* = k_k;\ D_k^* = D_k \qquad [50]$$

8. *Thermodynamic relations*

Under the assumption of interfacial thermodynamic equilibrium, the following conditions are valid at the solid/interdendritic liquid interface:

$$\overline{C}_e = \frac{T - T_m}{m_l} \qquad [51]$$

and

$$\overline{C}_{sd} = \begin{cases} \kappa\, \overline{C}_e & \text{during primary solidification} \\ C_s & \text{during remelting,} \end{cases} \qquad [52]$$

where it has been assumed that the remelting solid has a composition equal to the average concentration of the solid phase. The assumption eliminates the difficulties associated with determining the local composition of the solid that is remelting; however, establishing its validity clearly requires future experimental efforts.

IV. CONCLUSIONS

A multiscale/multiphase approach to modeling dendritic alloy solidification has been presented. The macroscopic transport equations are developed separately for the solid phase, the interdendritic liquid, and the extradendritic liquid using the technique of volume averaging. The model distinguishes different microscopic length scales present in a dendritic structure and links the microscopic phenomena occurring on each respective length scale to the heat flow, solute redistribution, melt convection, and solid movement taking place on the macroscopic (system) scale. In particular, the model incorporates the grain nucleation and dendrite growth mechanisms in addition to dendrite morphology and finite-rate solute diffusion in the solid. The model is intended for predicting compositional and structural features in an alloy casting. Representative numerical calculations for 2-D equiaxed dendritic solidification of an Al-4 wt pct Cu alloy are presented in part II, and some preliminary experimental validation is provided in part III.

NOMENCLATURE

A	interfacial surface area, m^2
A_s	area of the solid/interdendritic liquid interface, m^2
A_e	area of the dendrite envelope, m^2
$\mathbf{b}$	body force vector, N/m^3
C	concentration of a chemical species, wt pct
c	specific heat, J/kg K
C_ε	settling ratio
C_p	shape factor function
d_s	mean characteristic length or diameter of the solid phase, m
d_e	mean characteristic diameter of the dendrite envelope, m
D	mass diffusion coefficient, m^2/s
h	enthalpy, J/kg
Iv	Ivantsov function
j	species diffusion flux, kg/m^2 s
J	interfacial species transfer rate per unit volume
k	thermal conductivity, W/m K
l	species diffusion length, m
m_l	liquidus line slope, K/wt pct
$\mathbf{M}_s^d$	solid/liquid interfacial drag, N/m s
n	equiaxed nuclei density (m^{-3}), or an index in Eqs. [38] and [41]
$\mathbf{n}$	outwardly directed unit normal vector
Pe_ε	multiphase Pelcet number, $\varepsilon_l\lvert\mathbf{v}_l - \mathbf{v}_s\rvert d_e/D_l$
Pe_t	solutal Peclet number at the dendrite tip, $V_tR_t/2D_l$
Pe_∞	ambient Pelcet number for dendrite tips, $\lvert\mathbf{v}_l - \mathbf{v}_s\rvert R_t/D_l$
q	heat flux, W/m^2
Q	interfacial heat-transfer rate, W/m^3
R_t	tip radius
S	interfacial area concentration, A/V_0 (m^{-1})
Sc	Schmidt number, ν/D
t	time, s
T	temperature, K
$\mathbf{v}$	velocity vector, m/s
V_k	volume of phase k, m^3
V_0	averaging volume, m^3
V_t	dendrite tip velocity, m/s
w	interface velocity, m/s

Greek Symbols

β	dimensionless parameter, Eq. [38]
γ	momentum dispersion coefficient, Eq. [18]
Γ	interfacial phase change rate (kg/m^3 s) or Gibbs–Thomson coefficient (m K)
Γ^*	macroscopic transport property
Δh	latent heat of phase change, J/kg
ε	volume fraction
ε_{si}	internal solid fraction, $\varepsilon_s/(\varepsilon_s + \varepsilon_d)$
κ	partition coefficient, wt pct/wt pct
κ_v	flow partition coefficient
λ_2	secondary dendrite arm spacing, m
ϕ	sphericity
ρ	density, kg/m^3
μ	viscosity, Pa s
σ^*	stability constant
τ	shear stress
Φ	a general transfer
Ψ	a field property
Ω	solutal supersaturation, Eq. [30]

Subscripts

d	interdendritic liquid
e	dendrite envelope
E	eutectic
f	total liquid phase ($d + l$)

g	grain
j	phase j
k	phase k
kj	pertinent to phase k on the k-j interface
l	extradendritic liquid
ld	extradendritic-interdendritic liquid interface
m	melting point of pure metals
n	normal direction
N	nucleation
0	initial state
s	solid
sd	solid-interdendritic liquid interface
t	dendrite tip or tangential

Superscripts

c	critical
d	due to diffusion
j	due to species gradients
t	macroscopic dispersion
Γ	due to interface movement
$-$	interfacial area-averaged
*	effective

ACKNOWLEDGMENTS

This work was supported by the National Aeronautics and Space Administration under Grant No. NCC3-290.

REFERENCES

1. C.Y. Wang and C. Beckermann: *Metall. Trans. A*, 1993, vol. 24A, pp. 2787-2802.
2. F.P. Incropera and R. Viskanta: Paper presented at *Oji Int. Seminar on Advanced Heat Transfer in Manufacturing and Processing of New Materials*, Tomakomai, Hokkaido, Japan, Oct. 28–31, 1990.
3. M.C. Schneider and C. Beckermann: *Int. J. Heat Mass Transfer*, 1995, in press.
4. M. Rappaz: *Int. Mater. Rev.*, 1989, vol. 34, pp. 93-123.
5. Ph. Thévoz, J.L. Desbiolles, and M. Rappaz: *Metall. Trans. A*, 1989, vol. 20A, pp. 311-22.
6. V.R. Voller, M.S. Stachowicz, and B.G. Thomas: *Materials Processing in the Computer Age*, TMS, Warrendale, PA, 1991.
7. T.S. Piwonka, V.R. Voller, and L. Kategerman: *Modeling of Casting, Welding and Advanced Solidification Processes VI*, TMS, Warrendale, PA, 1993.
8. S.G.R. Brown and J.A. Spittle: *Mater. Sci. Technol.*, 1989, vol. 5, pp. 362-68.
9. P. Zhu and R.W. Smith: *Acta Metall. Mater.*, 1992, vol. 40, pp. 3369-79.
10. M. Rappaz and Ch.-A. Gandin: *Acta Metall. Mater.*, 1993, vol. 42, pp. 345-60.
11. C.Y. Wang and C. Beckermann: *Mater. Sci. Eng. A*, 1993, vol. A171, pp. 199-211.
12. C.Y. Wang and C. Beckermann: *Metall. Mater. Trans. A*, 1994, vol. 25A, pp. 1081-93.
13. J. Ni and C. Beckermann: *Metall. Trans. B*, 1991, vol. 22B, pp. 349-61.
14. C.Y. Wang and C. Beckermann: *Metall. Mater. Trans. A*, 1995, vol. 27A, pp. 0000-00.
15. C.Y. Wang and C. Beckermann: *Metall. Mater. Trans. A*, 1995, vol. 26A, pp. 0000-00.
16. C.Y. Wang: Ph.D. Thesis, The University of Iowa, Iowa City, IA, 1994.
17. M. Rappaz and Ph. Thévoz: *Acta Metall.*, 1987, vol. 35, pp. 1487-97.
18. H. Brenner and D.A. Edwards: *Macrotransport Processes*, Butterworth Scientific, London, 1993.
19. C.Y. Wang, S. Ahuja, C. Beckermann, and H.C. de Groh III: *Metall. Mater. Trans. B*, 1995, vol. 26B, pp. 111-19.
20. P.M. Adler: *J. Coll. Int. Sci.*, 1981, vol. 81, pp. 531-35.
21. D.M. Stefanescu, G. Upadhya, and D. Bandyopahyoy: *Metall. Trans. A*, 1990, vol. 21A, pp. 997-1005.
22. J. Lipton, M.E. Glicksman, and W. Kurz: *Mater. Sci. Eng.*, 1984, vol. 65, pp. 57-63.
23. C.Y. Wang and C. Beckermann: in *Micro/Macro Scale Phenomena in Solidification*, C. Beckermann, H.P. Wang, L.A. Bertram, M.S. Sohal & S.I. Guceri, eds., ASME, New York, NY, 1992, ASME HTD-vol. 218/AMD-vol. 139, pp. 43-57.
24. S.C. Huang and M.E. Glicksman: *Acta Metall.*, 1981, vol. 29, pp. 701-15.
25. R. Ananth and W.N. Gill: *J. Cryst. Growth*, 1991, vol. 108, pp. 173-89.
26. P.C. Carman: *Flow of Gases through Porous Media*, Butterworth Scientific, London, 1956.
27. M.C. Flemings: *Solidification Processing*, McGraw-Hill, New York, NY, 1974.
28. J. Happel and H. Brenner: *Low Reynolds Number Hydrodynamics*, Noordhoff International Publishing, 1976.
29. H.C. de Groh III, P.D. Weidman, R. Zakhem, S. Ahuja, and C. Beckermann: *Metall. Trans. B*, 1993, vol. 24B, pp. 749-53.
30. S. Ahuja: Master's Thesis, The University of Iowa, Iowa City, IA, 1992.
31. P.K. Agarwal: *Chem. Sci. Eng.*, 1988, vol. 43, pp. 2501-10.
32. J. Ni and C. Beckermann: *J. Mater. Processing Manufacturing Sci.*, 1993, vol. 2, pp. 217-31.
33. A. Ramani: Master's Thesis, The University of Iowa, Iowa City, IA, 1995.
34. R.H. Davis: *Adv. Colloid Interface Sci.*, 1993, vol. 43, pp. 17-50.
35. I.M. Krieger: *Adv. Colloid Interface Sci.*, 1972, vol. 3, pp. 111-36.
36. M.C. Flemings: *Metall. Trans. A*, 1991, vol. 22A, pp. 957-81.
37. L. Arnberg, G. Chai, and L. Backerud: *Mater. Sci. Eng.*, 1993, vol. A173, pp. 101-03.